

Operation Regime of a High β Low q Tokamak Plasma

Hiroko KIYAMA and Satoru KIYAMA

In this paper, we will explain the operation regime of high β low q tokamak plasmas, which were produced by a fast screw pinch machine (TPE-2). In the Hugill diagram, the normalized electron density ($\bar{n}_e R/B_t$) is maximum near $q_t=1.5-1.6$ and 3. The particle losses at the relaxation phenomena may mainly determine the maximum density. The particle flow related to q_t is discussed. In these plasmas the current disruption was not observed generally. In order to make the current disruption, a high error field is supplied from the toroidal shell gap. The plasma rotation is important to avoid the disruption as same as the usual tokamaks.

§1 Introduction

Studies of operating regimes of plasma discharges have been done for all tokamaks. The tokamak operation regimes, which are a relation of the normalized plasma current and the normalized density, have been distinguished by four limits, that is, 'Murakami limit'⁽¹⁾, 'Hugill limit'⁽²⁾, 'low q limit' and 'Runaway limit'. q is the safety factor. These limits define the Hugill diagram. The Murakami limit, that is, the highest density achievable was determined by a balance between input power and radiated power. The maximum density: n_{max} increases with reducing the radiation loss and with increasing input power. In the Hugill density limit, where the Murakami number ($\bar{n}_e R/B_t$, \bar{n}_e : the averaged electron density, R : the major radius, B_t : the toroidal magnetic field) is a linear relation of $1/q_t$ (q_t : the current q), n_{max} is proportional to the plasma current: I_p , ($n_{max} \propto I_p$) and it does not depend on input power. Many papers reported that the Hugill limit may be due to a deterioration of particle confinement in the core plasma⁽³⁾, or due to the MHD unstable current distribution by the increase in impurity radiation with increasing density⁽⁴⁾. The low q limit is a MHD stability limit and this occurs at $q=1$. Furthermore, there are another limits such as β_p , β_t limit due to MHD instabilities, and the disruption by locked

mode. These operation regions were generally obtained in plasmas where the discharges start from the low-density plasmas (low Murakami number) and the densities increase by gas puffs. As the densities increase at first from the edge region by the gas puffs, the current distribution tends to contract. Then, if the high density and high temperature plasmas are produced in a short time by higher power heating than the Ohmic heating, the operation regime may be expanded. The screw pinch plasma⁽⁵⁻⁹⁾, was produced by implosion heating, that is, by ramping up the toroidal and the poloidal field simultaneously in 2.8 μ s from the preheat plasma with the low toroidal field. It has the feature that the plasma is completely ionized by the high input power and exceeds the radiation barrier except high-density plasma, and then the discharge starts from high Murakami number. Furthermore, the initial electron density profile is peaked. Then, the time variation of the profile is supposed to resemble that of the pellet injection. As the recycling rate at the wall is about 0.3-0.4^(10,11), the plasmas are produced without gas puff and the discharge duration is short, the wall has the ability to absorb particles sufficiently during the discharge. While, in this plasma, just after the implosion heating, high β very low q tokamak plasma with an inherent q profile is self-organized rapidly through a relaxation process⁽⁸⁾. In the

KEY WORDS : plasma, high β plasma, low q tokamak plasma, operation regime, density limit, q limit, disruption, rotation

relaxed state, the current distribution is broad, then the central q : $q(0)$ is not 1 but close to q_I . Then, the low q limit may occur at $q_I \sim 2$ and $q_I \sim 1$. As B_t or I_p can be changed quickly in this experiment, we can observe the dynamic change of the electron density. Therefore, the operation regime in this plasma is expected to be quite different from the usual tokamaks. The plasmas may be effective to know physical process of the operation limit. In this paper, we explain the operation regime of high β low q tokamak plasmas which were produced by the fast screw pinch machine (TPE-2)⁵⁻¹¹. The operation regime is given in the section 2. The particle flow to the edge and the relation to q are explained in the section 3. The phenomena near the low q limit are given in the section 4. The effect of the error field on the plasma disruption by supplying an external field at the toroidal shell gap is given in the section 5. The discussion and the conclusion are given in the section 6.

§2 Operation Regime

TPE-2 is a toroidal screw pinch device with an elongated cross section ($b/a=0.21$ m / 0.13 m, $\kappa=1.6$, $A=3.5$, deuterium plasma) and with a conducting shell⁵. The wall surface was pre-coated by titanium. Helium discharge cleaning was done between every main discharge to desorb D atoms from the surface, which were absorbed during the former discharge. The estimated recycling rate is about $0.3-0.4$ ^{10,11}. High β plasmas were produced by ramping up the toroidal and poloidal magnetic fields simultaneously in 2.8 μ s. The initial plasmas ($\bar{n}_e > 10^{20}/\text{m}^3$, $T_i \geq T_e > 50-100$ eV) are completely ionized by the high input power and exceed the radiation barrier except high-density plasmas. The plasmas are further heated by the joule heating ($\bar{n}_e \sim 0.3-2.0 \times 10^{20}/\text{m}^3$, $T_i \sim T_e \sim 100-300$ eV). High β very low q tokamak plasmas with an inherent q profile were self-organized rapidly through a relaxation process⁸. In the relaxed plasmas, the current distribution is broad, then $q(0)$ is close to q_I . The necessary condition for relaxation to the high β low q stable state is that $\beta_p > 0.6$ and the plasmas rotate¹². The magnetically deformed plasmas

rotate. The rotating speed of the mode decreases with increasing of q_I and \bar{n}_e ^{12,13}. Here, the current q_I is defined as $q_I = (l_p^2 / 2\pi R_0) B_t / \mu_0 I_p$. In this experiment, l_p is defined as the peripheral poloidal length of the last closed flux surface.

Time variations of the plasma parameters of typical high q plasma ($q_I > 2$) with relaxation phenomena are shown in **Fig.1**. In this case, $q_I = 2.4-2.7$. Where we define the relaxation phenomena as the internal disruption at $q(0)=1, 2$ and 3 and the reconnection at $q(r)=2$ and 3 surface near the edge of the core plasma. B_t , I_p , q_I , $n \cdot l$ at 4 positions, the volume averaged density \bar{n}_e , the surface voltage V_s , D_β , Soft X-ray signal of a low energy part, the edge density near the wall j_s , the radiation loss powers P_{rad} at the plasma center and the edge, and the total loss power measured from the thermal flux are shown. Here, the averaged density \bar{n}_e was estimated from $n \cdot l$ data, which were obtained by four channels CO₂ interferometer. j_s is the ion saturation current of the double probes at 5 mm inside from the wall ($\rho=125$ mm). The low energy Soft X-ray signal was obtained by a diode through 2 μ m Aluminum film. The signal was measured viewing the horizontal chord. The radiation loss powers were measured by 5 channels Bolometer viewing the vertical chord, and the data of the 2 channels are shown in the figure. The overall gas absorption values on the wall were measured by a diaphragm pressure gauge. In the measurement, the gas pressure was measured just before, during and just after the discharge as the filling gas is absorbed during the discharge. From the decrement of the pressure, we obtained the global absorption rate of the wall and estimated the global recycling rate of the discharge^{10,11}. The D₂ gas absorption rate was 0.7 during this discharge. I_p slightly decreases or remains constant, even though V_s is negative in B_t decaying phase ($t=0.7-0.87$ ms). The electron density profile is peaked initially by the implosion heating. \bar{n}_e becomes a nearly steady value in 5-10 μ s and it decreases gradually until B_t decaying phase ($t=0.7$ ms). The radiation loss power of the core plasma is nearly constant in the steady state. However, at the relaxation phenomena, the edge radiation power

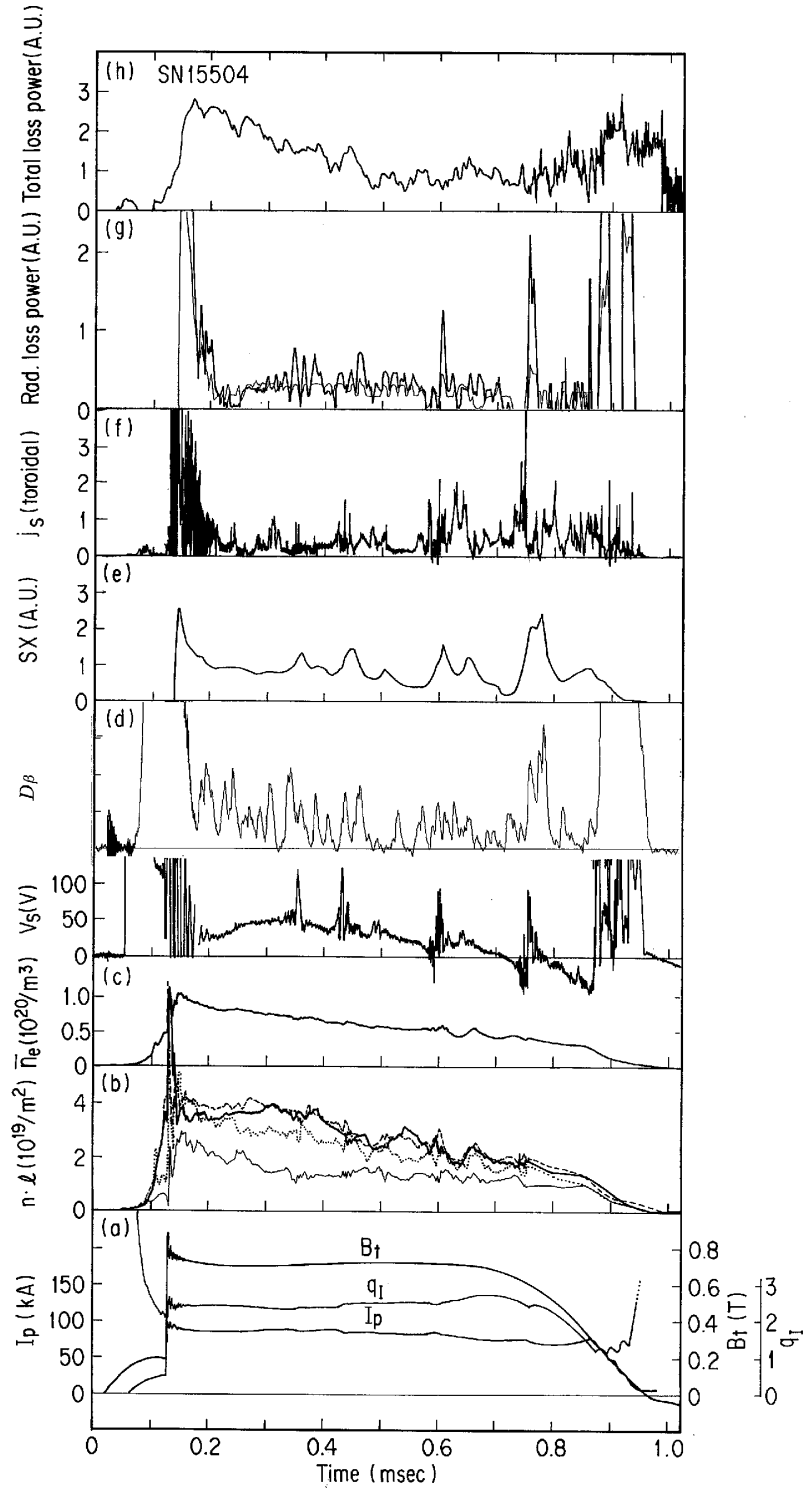


Fig.1 Typical time variations of the plasma parameters of plasma with the relaxation oscillation.

(a) B_t , I_p , q_I . (b) $n-l$ of 4 vertical chords at -3 cm, 0 cm, +3 cm and +6 cm from the magnetic axis are shown by a solid line, a broken line, a dotted line and a thin line, respectively. (c) The volume averaged density \bar{n}_e . (d) The surface voltage V_s and $D\beta$. (e) The Soft Xray signal of a low energy part. (f) The ion saturation current of the electro-static double probes at the edge plasma near the wall j_s . (g) The radiation loss powers at the plasma center and at the edge of the core plasma are shown by a thin line and a thick line, respectively. (h) The total loss power measured from the thermal flux is shown. The delay time of the thermal flux measurement is about 20~60 μ s.

increases intermittently and pulsively with V_s , j_s and the Soft X-ray also increase with V_s simultaneously. The density profile ($n \cdot l$) changes considerably, while \bar{n}_e decreases slightly at the same time, sometimes with steps.

In this case, the decay time of \bar{n}_e is about 0.6 ms, while that of \bar{n}_e without relaxation phenomena is 1-5 ms. In B_t decaying phase, from $t=0.78$ ms, q_I decreases gradually and the energy flow (the total loss power) increases. From $t=0.88$ ms, q_I is close to 1, the edge radiation loss power increases suddenly and j_s near the wall increases, then the plasma current decreases with steps so as to keep q_I about 1.

The typical time variations of q_I and \bar{n}_e are shown by the trace of $\bar{n}_e R/B_t - 1/q_I$ in Fig.2. The traces are plotted for the various discharge modes, that is, a high q mode (the plasma current is roughly constant at $q_I > 2$ from the time of the implosion heating until the time of B_t decaying phase, as shown in Fig.1), a low q mode (the plasma current is roughly constant at $q_I < 2$), a ramp up mode (the plasma current ramps up from $q_I > 2$ to $q_I < 2$) and a slow screw pinch mode (the rise time is 0.2-0.5 ms, $q_I < 2$). The starting times of two traces (ramp up mode, slow screw pinch mode) begin just after the pre-heat, that is, from the onset of the implosion heating, in the figure. The traces during the implosion time of the other cases are neglected in the figure. In contrast to the usual tokamaks, the discharges start from high $\bar{n}_e R/B_t$,

vary with $\bar{n}_e R/B_t - 1/q_I$, stay in nearly steady state with some q_I and \bar{n}_e values, and stay at $q_I \sim 1.2$ from 0.87 ms in the B_t decaying phase (as shown in Fig.1) and finish. In the B_t decaying phase, $1/q_I$ increases with constant $\bar{n}_e R/B_t$, and at last the plasma decays at $q_I = 1.2$. In the slow screw pinch mode, \bar{n}_e increases with increasing B_t during the rise time, just after the pre-heat. On the other expression, as $1/q_I$ is nearly constant with constant $\bar{n}_e R/B_t$ just after the initial variation, the density \bar{n}_e increases with increasing the current I_p . In the usual tokamak mode of the TPE-2 experiment, the discharge started from low $\bar{n}_e R/B_t$ and $1/q_I$ (the rise time 0.2 ms, $q_I > 3$) and $1/q_I$ increased linearly with $\bar{n}_e R/B_t$, as the usual tokamaks.

The normalized current: $1/q_I$ in the nearly steady state in Fig.2 are plotted versus the normalized density: $\bar{n}_e R/B_t$ for many discharges of various discharge modes in Fig.3. $1/q_I$ values of the high q mode ($q_I > 2$, \square), the low q mode ($q_I < 2$, \times), the ramp up mode ($q_I < 2$, \square) and the B_t, I_p up mode ($q_I < 2$, \triangle) are plotted against $\bar{n}_e R/B_t$. In these plots, the nearly steady state values of \bar{n}_e for the ramp up mode and the B_t, I_p up mode are plotted when q_I becomes the steady state after I_p ramps up.

The operation diagram seems to be different from the regimes of general tokamaks, which are distinguished by four limits. The features of the two figures are summarized as follows;

- (1) There is the maximum density depending on $1/q_I$.

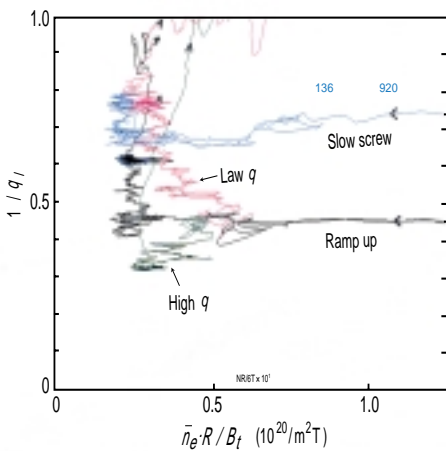


Fig.2 The typical time variations of q_I and \bar{n}_e are shown by the trace of $\bar{n}_e R/B_t - 1/q_I$. The traces are plotted for the various discharge modes, that is, a high q_I mode, a low q_I mode, a ramp up mode and a slow screw pinch mode.

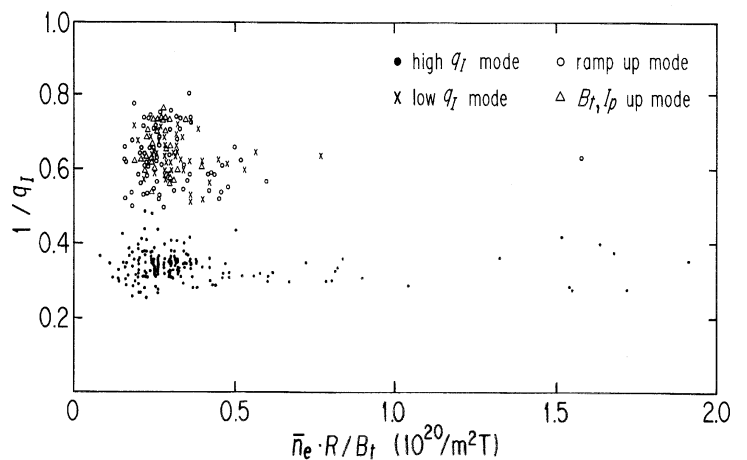


Fig.3 The Hugill plots of q_I and the normalized density $\bar{n}_e R/B_t$ in the relaxed steady state are shown for various discharge modes. High q_I mode (\square), low q_I mode (\times), ramp up mode (\square) and B_t, I_p up mode (\triangle).

Larger values of $\bar{n}_e R/B_t$, appear near $q_I=1.5-1.6$ and 3, that is, there are windows of the density near $q_I=1.5-1.6$ and 3. There are discontinuities at $q_I=1.2$ and 2 in the diagrams. The maximum $\bar{n}_e R/B_t$ increases with decreasing of q_I for $q_I>3$ and decreases with decreasing of q_I for $2<q_I<3$. Furthermore, it increases with decreasing of q_I for $2>q_I>1.5$ and decreases with decreasing of q_I for lower q_I .

- (2) A linear dependence of $\bar{n}_e R/B_t$ on $1/q_I$ of the maximum density is not clear. The current disruption by the Hugill density limit was not observed. The reason is that the discharges have no gas puffing and the low recycling surface, and the discharge duration is short.
- (3) $\bar{n}_e R/B_t - 1/q_I$ traces in the initial time of the discharges, as shown in Fig.2, seem to move dynamically in the operation regions in Fig.3. In the high q mode of $q_I\sim 3$ or the low q mode of $q_I\approx 1.5-1.6$, \bar{n}_e is almost constant during the discharge after initial phase, while, in the ramp up mode or in the case that q_I is varied, \bar{n}_e decreases with decreasing of q_I during the discharge except the windows.
- (4) The lowest q_I ($q_I\approx 1.2$) is achieved in low-density plasmas.
- (5) In the B_t decaying phase, q_I decreases with constant $\bar{n}_e R/B_t$. The pure current disruption was not observed.
- (6) At high density plasmas : $\bar{n}_e > 1.2 \times 10^{20}/\text{m}^3$ ($\bar{n}_e R/B_t > 0.7 \times 10^{20}/\text{m}^3$, at $q_I\sim 3$), I_p and \bar{n}_e decay severely during the discharge, however, the decay constant of the density becomes longer when V_s is increased so as to sustain the plasma current constant, that is, Ohmic input power is increased. This limit is due to the radiation loss and the core radiation became important loss⁸⁾. The highest Murakami number ($\bar{n}_e R/B_t$) is $1.8 \times 10^{20}/\text{m}^3\text{T}$, which is obtained only at $q_I\sim 3$.
- (7) In the B_t, I_p up mode, $\bar{n}_e R/B_t$ and $1/q_I$ are nearly constant or decrease slightly with B_t increasing during the discharge. The value of \bar{n}_e moves in the region of the diagram.

- (8) Higher densities were obtained in helium plasma. Lower densities were obtained in hydrogen plasma. The values of $\bar{n}_e R/B_t$ were still in the region of the diagram.

In conclusion, there are windows for the density at $q_I=1.5-1.6$ and 3 in the $\bar{n}_e R/B_t - 1/q_I$ traces. Then, it is thought that the particle loss depends on q_I and determines the maximum density. The Murakami limit is obtained only at $q_I\sim 3$. Perhaps the value at $q_I\sim 1.5-1.6$ may be one of the Murakami limit as the density profiles are different in the two regions.

§3 Particle Confinement

The Hugill diagram of the experiment suggests that the particle confinement deteriorates except the windows near $q_I\sim 1.5-1.6$ and $q_I\sim 3$. It is considered that these windows of $q_I\sim 1.5-1.6$ and $q_I\sim 3$ may result from the inherent profile of the high β low q tokamak plasma and the causes may be due to the relaxation phenomena by the MHD activity or to fluctuations. In the relaxation transition, $V_s, j_s, D\beta, \text{Soft Xray}$ and P_{rad} at the edge increase pulsively at $t=0.36, 0.43, 0.60, 0.76$ ms, as shown in Fig.1 and a part of the particles and the energy are lost. The relaxation phenomena occur intermittently. We define it as relaxation oscillation. In this section, we will explain about the particle confinement in the plasmas near the window and the relation of the relaxation oscillation. We will discuss what process determines the density considerably less than the Murakami limit.

3.1 Particle flow

The density and the temperature of the edge plasma were obtained by the two pairs of the electro-static double probes. The double probes were placed nearly parallel and perpendicularly to the magnetic field. The example of the ion saturation currents (j_s) of the double probes in the edge is shown in Fig.1. Here, we assume that the particle flow is related to j_s at the edge, therefore, \bar{j}_s / \bar{n}_e should be related to the global out-flow velocity to the edge. The assumption may be right if the recycling

rate of the wall is low. However, if the recycling rate is high (~ 1) as in the usual tokamaks, the influx from the wall may determine the electron density. There, the decay time of the electron density must increase by increasing of the influx, even though the out flux decreases. In this experiment, the assumption is right as the overall recycling rate is about 0.3-0.4. Here, \bar{j}_s is the averaged value of the steady state during 0.1 ms at plasma edge near the wall (5 mm inside from the wall). \bar{j}_s / \bar{n}_e versus $1/q_l$ are plotted for the high q mode and the low q mode, and the ramp up mode, as shown in Fig.4a and 4b, respectively. The parameters are \bar{n}_e of the steady state. The figures were obtained in the case of initial filling pressure of 2.5 mTorr in the high q mode and the ramp up mode, and of 2 mTorr in the low q mode. As the filling gas was completely ionized by pre-heat, the initial \bar{n}_e is almost same, however, \bar{n}_e of the steady state changes depending on q_l or discharge mode, as shown in Fig.2 and 3. \bar{j}_s / \bar{n}_e is minimum near $q_l \sim 1.5-1.6$ and 3 for each \bar{n}_e . Then, it is suggested that near $q_l \sim 1.5-1.6$ and 3, the global out-flow velocity to the edge decreases comparing with the other q_l regions. In a different expression, the particle confinement deteriorates except the region near $q_l \sim 1.5-1.6$ and 3. Then, Murakami number is maximum near $q_l \sim 1.5-1.6$ and 3.

The typical density profile in the steady state of a ramp up mode and the profile of a ramp up failure mode are shown in Fig.5a. Here, the ramp up failure mode is the mode that the plasma current cannot increase to $q_l < 2$ when the current is increased and q_l stays close to 2 or over. The profile of the ramp up failure mode is peaked, but it is transit. It becomes hollow at the relaxation transition. The density profile at the transition of a relaxation oscillation is also shown in the figure. Here, the core electron densities are the line averaged densities and were obtained from $n l$ and the edge densities are local values and were obtained from the electro-static double probes. They were obtained at the same toroidal position. At the transition, j_s increases at the edge and a certain number of particles are lost. Just after the transition, the profile returns the original steady state one. In the ramp up failure mode, the peaked profile

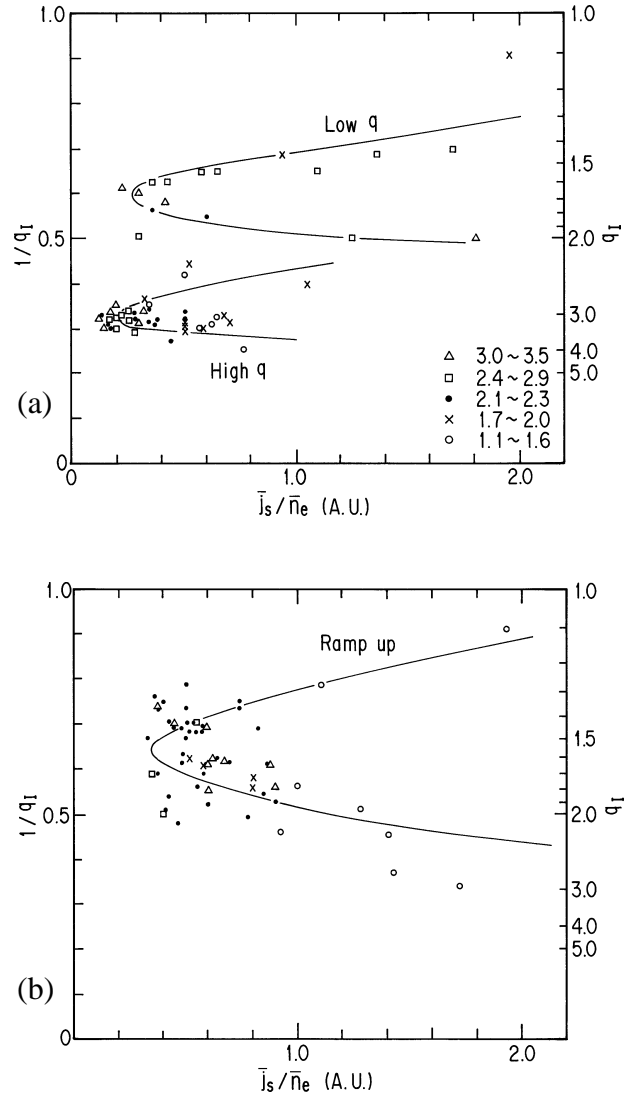


Fig.4 a \bar{j}_s / \bar{n}_e versus $1/q_l$ are plotted for the various \bar{n}_e in the relaxed steady state of the high q_l mode and the low q_l mode. Here, the values of the parameters of \bar{n}_e in the figure must be multiplied by $2.5 \times 10^{19} / \text{m}^3$. (: $(7.5-8.8) \times 10^{19} / \text{m}^3$, : $(6.0-7.3) \times 10^{19} / \text{m}^3$, : $(5.3-5.8) \times 10^{19} / \text{m}^3$, x: $(4.3-5.0) \times 10^{19} / \text{m}^3$, : $(2.8-4.0) \times 10^{19} / \text{m}^3$.) In these plots, the \bar{n}_e just after the implosion heating is almost the same. b \bar{j}_s / \bar{n}_e versus $1/q_l$ are plotted for the various \bar{n}_e of the ramp up mode.

and the hollow profile at the transition were observed 2-5 times repeatedly near $q_l \sim 2$, and a large number of particles were lost. $n_e(0) / \bar{n}_e$ in the steady state are plotted against q_l , as shown in Fig.5b. The density profile depends on q_l , that is, it is sharper with q_l , and in detail, the profile seems to be sharper near $q_l \sim 1.5-1.6$ and 3. It may be concluded that the global particle flow to the edge decreases near $q_l \sim 1.5-1.6$ and 3 than the other region, and the sharper density profile is established,

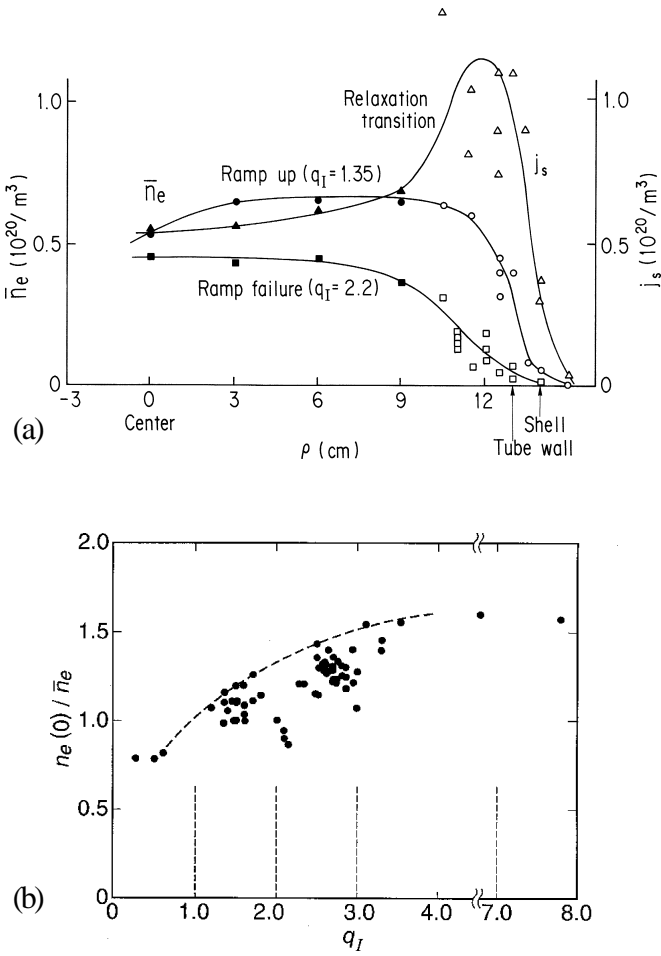


Fig.5 a The typical density profile in the steady state of a ramp up mode and the profile of a ramp up failure are shown. The density profile at the transition of a relaxation oscillation is also shown. Here, the core electron densities are the line averaged densities and were obtained from $n \cdot l$ and the edge densities are local values and were obtained from the electrostatic double probes.
 b $n_e(0)/\bar{n}_e$ in the relaxed state are plotted against q_I .

then, \bar{n}_e becomes maximum in the windows.

3.2 Recycling

As D_α is related to the influx of D atoms from the wall, \bar{D}_α/\bar{n}_e should be related to the global influx velocity. \bar{D}_α/\bar{n}_e and \bar{D}_β/\bar{n}_e for each mode (, : high q mode, , : low q mode, , : ramp up mode) are plotted versus $1/q_I$, as shown in Fig.6. At near $q_I \sim 1.5-1.6$ and 3 ($1/q_I \sim 0.65$ and 0.35), the influx \bar{D}_α/\bar{n}_e and \bar{D}_β/\bar{n}_e decreases. They are small especially in the low q mode. These results suggest that the decrement of the particle influx in the widows is due to the decrease of the outflow of the

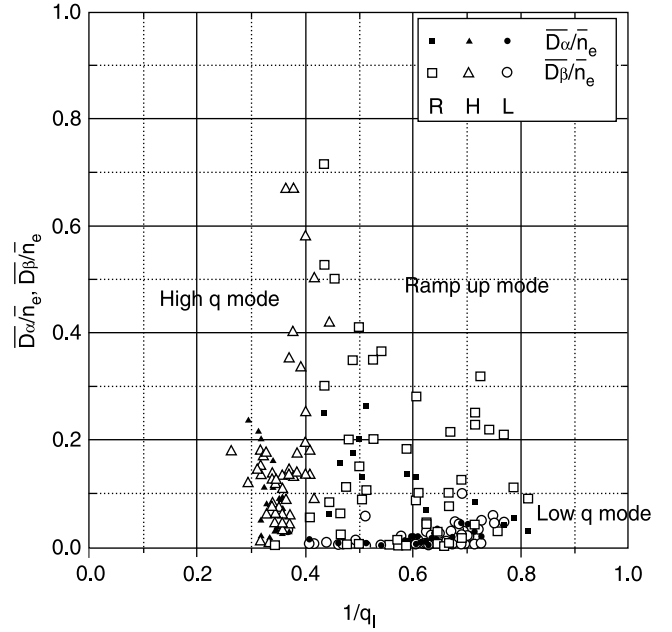


Fig.6 \bar{D}_α/\bar{n}_e and \bar{D}_β/\bar{n}_e are plotted against $1/q_I$ for the high q mode, the low q mode and the ramp up mode.

particles.

As j_s is related to the outflow from the core plasma and D_α is related to the influx from the wall, \bar{D}_α/\bar{j}_s should be related to the recycling rate of the wall. \bar{D}_α/\bar{j}_s and \bar{D}_β/\bar{j}_s for the high q mode (: \bar{D}_α/\bar{j}_s , : \bar{D}_β/\bar{j}_s), the low q mode (: \bar{D}_α/\bar{j}_s , : \bar{D}_β/\bar{j}_s) and the ramp up mode (: \bar{D}_α/\bar{j}_s , : \bar{D}_β/\bar{j}_s) are plotted versus $1/q_I$, as shown in Fig.7a, b. \bar{D}_α/\bar{j}_s and \bar{D}_β/\bar{j}_s also decreases at $q_I \sim 1.5-1.6$ and 3. This means that the influx increases more than the outflow increment in the region of q_I except $q_I \sim 1.5-1.6$ and 3. In these windows, the particle out flux decreases, as the results, the influx decrease much more. In high recycling wall, the windows of \bar{D}_α/\bar{j}_s were not seen. The high recycling may cover the q_I dependence.

\bar{D}_β/\bar{j}_s at $q_I \sim 1.5-1.6$ and 3 are plotted against \bar{n}_e in Fig. 7c. Here, \bar{n}_e was increased with increasing of the filling pressure. The values increase suddenly when $\bar{n}_e > 10^{20}/m^3$. The recycling rate increases at the high filling gas pressure and the high-density plasma. The wall may not have the capacity to absorb the gas in the high filling gas.

The global absorption rate depends on the phenomena of the discharge. The absorption rate: $\delta p/p$ of the ramp up mode is plotted versus the filling pressure: p in Fig.8a. The absorption rate is low at the low filling pressure, increases with p , maximum at 3.5 mTorr and

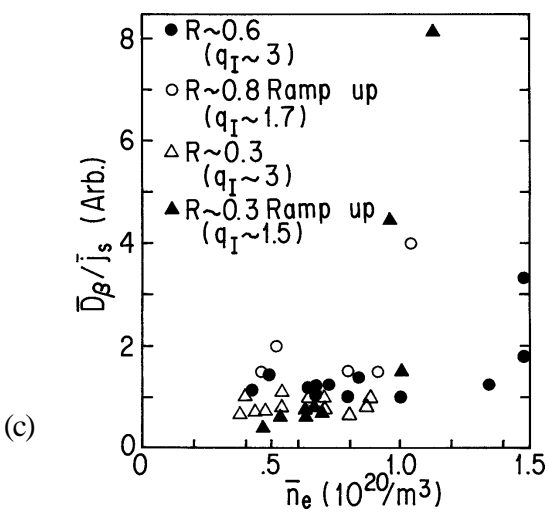
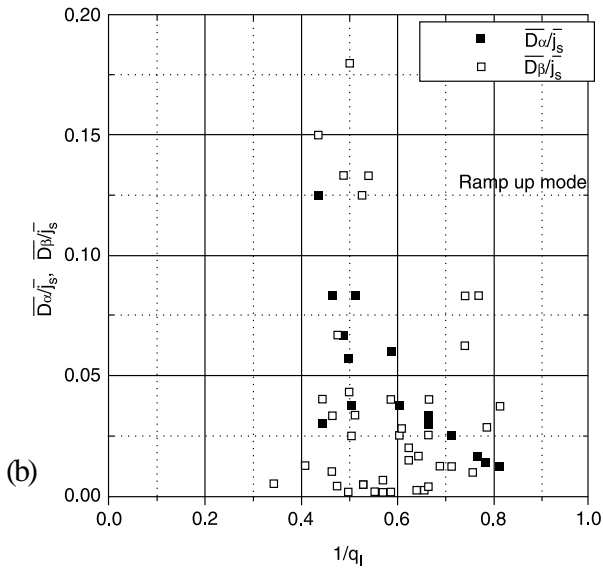
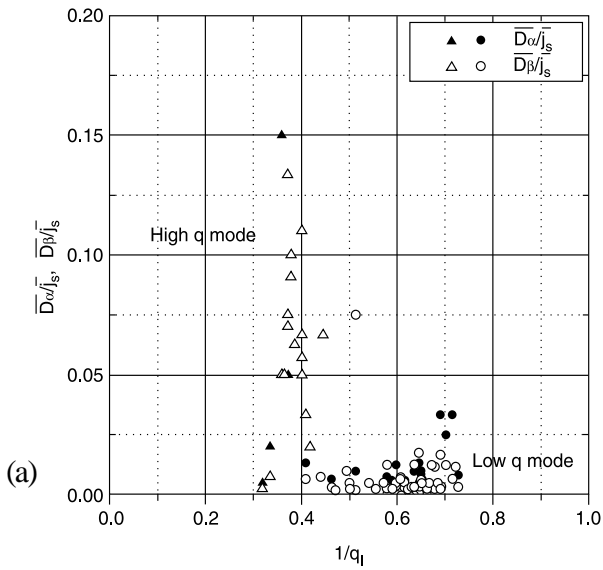


Fig.7 a $\bar{D}_{\alpha}/\bar{j}_s$ and $\bar{D}_{\beta}/\bar{j}_s$ for the low q mode and the high q mode are plotted against $1/q_I$. b $\bar{D}_{\alpha}/\bar{j}_s$ and $\bar{D}_{\beta}/\bar{j}_s$ for the ramp up mode are plotted against $1/q_I$. c $\bar{D}_{\beta}/\bar{j}_s$ for $q_I \sim 3$ (the recycling rate : $R \sim 0.6$ and 0.3) and for $q_I \sim 1.7-1.5$ ($R \sim 0.8$ and 0.3) are plotted against \bar{n}_e .

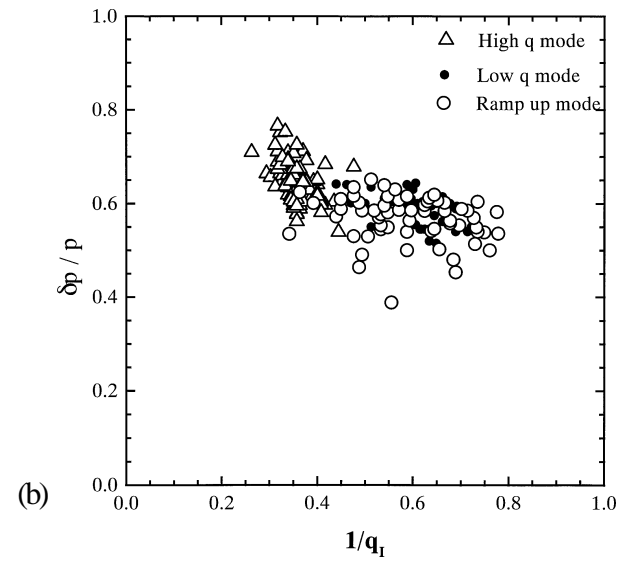
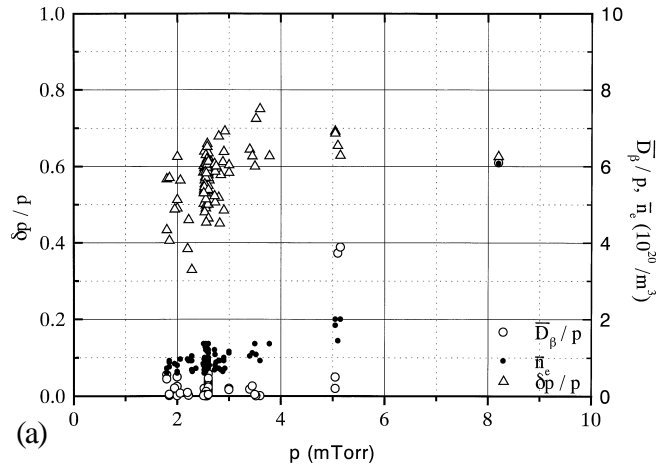


Fig.8 a $\delta p/p$, \bar{D}_{β}/p and \bar{n}_e of ramp up mode are shown against p . b $\delta p/p$ are plotted against $1/q_I$ for the high q mode, the low q mode and the ramp up mode.

decreases at higher p . \bar{n}_e at the steady state are plotted against p in the figure. \bar{n}_e is roughly proportional to the filling pressure. The inclination of \bar{n}_e to p is higher at $p > 5$ mTorr. \bar{D}_{β}/p are also plotted in the figure. \bar{D}_{β}/p increase drastically from $p > 5$ mTorr, that is, the influx increases. From the pressure, $\delta p/p$ decreases. The absorption rate of the wall decreases and then the recycling rate increases, as the result, \bar{n}_e increases. The scatter of the data depends on the phenomena. $\delta p/p$ of the high q mode, the low q mode and ramp up mode are plotted against q_I , as shown in Fig.8b. $\delta p/p$ is large at $1/q_I \sim 0.3$ and decreases with increasing $1/q_I$. This graph is consistent with the recycling rate in Fig.7a,b.

3.3 The relaxation oscillation

The relaxation phenomena are supposed to cause mainly the particle loss, as described in 3.1. At the transition of a relaxation oscillation, the one-turn voltage V_s changes quickly, and the edge particle flows (j_s) and the edge radiation power increase, as shown in Fig.1. In this plasma, $q_I=2.4-2.7$ and $q(0)$ is close to 2. The time variations of q profile near a relaxation transition are shown in **Fig.9**. Here, the q profile was obtained from the peripheral poloidal magnetic fields around the plasma⁵⁾. The fields were measured by 12 magnetic coils on the inner surface of the shell. The sets of the coils around the poloidal direction were placed also at 6 toroidal directions. Here, in this estimation, the uncertainties in $q(\psi)$ are less than 10 % at the edge plasma and that are about 20 % at 70% of $q(\psi)$, but the uncertainties are greater than 50 % at the center of the plasma. At each transition, the small internal disruption occurs, as shown in Fig.9. Near the transition ($t=0.576-0.590$ ms), at first, q profile (at $t=0.576$ ms) becomes gradually broader than the relaxed one (at $t=0.560$ ms), that is, the current density profile becomes broad, and then, V_s decreases (for example, 0.58-0.59 ms in Fig.1). At the time, the core density profile seems to be broad or hollow and j_s increases. After a few μ s, V_s and j_s

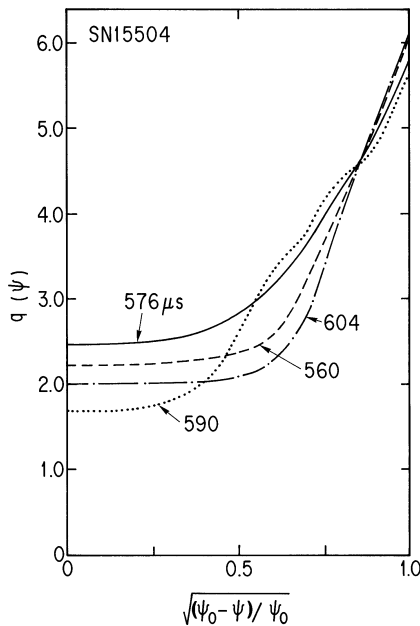


Fig.9 The time variations of q profile near a relaxation transition are shown.

quickly increase. The reconnection may occur at $t=0.590$ ms. A certain number of particles are lost from the edge plasma, as shown in Fig.5a. The plasma energy is also lost. Then, the averaged density decreases sometime with step. Finally, the q profile returns to the original relaxed one (at $t=0.604$ ms) in about 10-20 μ s. This event is repeated.

The periods of these events depend on q_I . The period of between 2 events (the period between a relaxation to the next relaxation) is plotted against q_I in **Fig.10**. The periods increase roughly with q_I , however, that are long at $q_I \sim 1.6$ and 3, and are short extremely near $q_I \sim 2$. When q_I decreases to 2, V_s and j_s change more violently near $q_I \sim 2$. Then, the particles and the energy are lost violently and the confinements are more deteriorated. When q_I is close to 3, the periods increase more than 0.3-0.5 ms, then, the relaxation oscillations disappear in many cases and the particle confinement increase than the other region. The high Murakami numbers are obtained when q_I is nearly 3 after the initial relaxation. When q_I is decreased from 2 close to 1, the periods further decrease. When q_I approaches to the low q limit, the periods are shorter than 50 μ s and the particles and energy are lost violently.

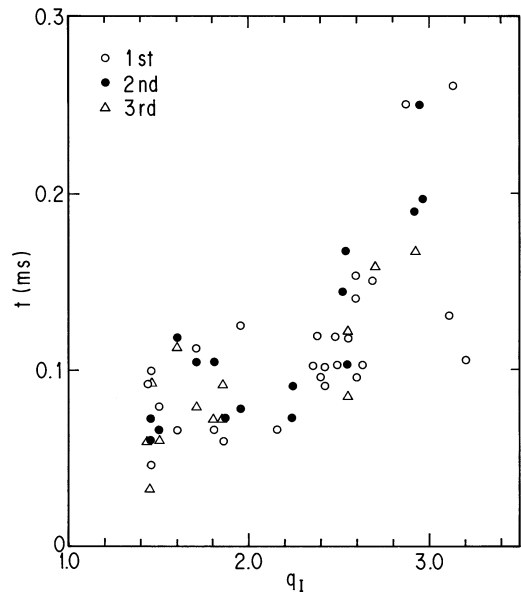


Fig.10 The periods of between a relaxation to the next relaxation are plotted against q_I . The periods of the 1st, the 2nd and the 3rd relaxation are shown by \circ , \bullet , and \triangle , respectively.

The high Murakami numbers are also obtained in the ramp up mode, especially in the low q mode. In the low q mode, q_I is nearly 1.5-1.6 after the initial relaxation and the period of it is longer. The density profile is rather peaked. The high particle confinement is obtained. At $q_I=1.5-1.6$, a small relaxation oscillation still occurs. In the case, sometimes, the relaxation occurs at the local region in the toroidal direction, and then we cannot observe the events at the different measurement ports. By the reason, we plotted the data of the steady state and averaged values included the relaxation in Fig.3 and Fig.4. At the relaxation transition, at first, q profile has a step near the surface of $q=2^{(10)}$, which locates near the edge of the core plasma, and the step disappears quickly. At the time, the particle flow and the energy flow also occur suddenly, and then, the profile regimes to the relaxed one.

Therefore, it is suggested that the relaxation oscillation limits mainly the particle confinement and the operation regimes.

§4 Low q Disruption

When the plasma current increases and q_I decreases less than 1.2, the central q is less than 1. $n=1$ internal mode occurs. The plasma current decays a few % and the density decreases a few % in a few μs . It is the low q limit in this experiment. After that, the relaxed profile is reconstructed. Then, the current stays above the low q limit. This phenomenon is almost the same as sawtooth relaxation in tokamaks. However, in contrast to the general tokamaks, from the reason of broad current density, the plasma surface q : q_a is less than 2, and then, the inner disruption contacts directly to the wall.

The phenomena of the low q limit are clearer in B_t decaying phase, as shown in Fig.11a and 11b. In the trace of $\bar{n}_e R/B_t - 1/q_I$ in Fig.2, $1/q_I$ increase with constant $\bar{n}_e R/B_t$ and at last the plasma terminates at $q_I=1.2$. When B_t decreases from $t=0.7$ ms at the low q plasmas ($q_I < 2$), I_p remains almost constant for a while even though V_s is negative, and therefore, q_I decreases directly. In detail, as the plasma internal inductance l_i is almost constant,

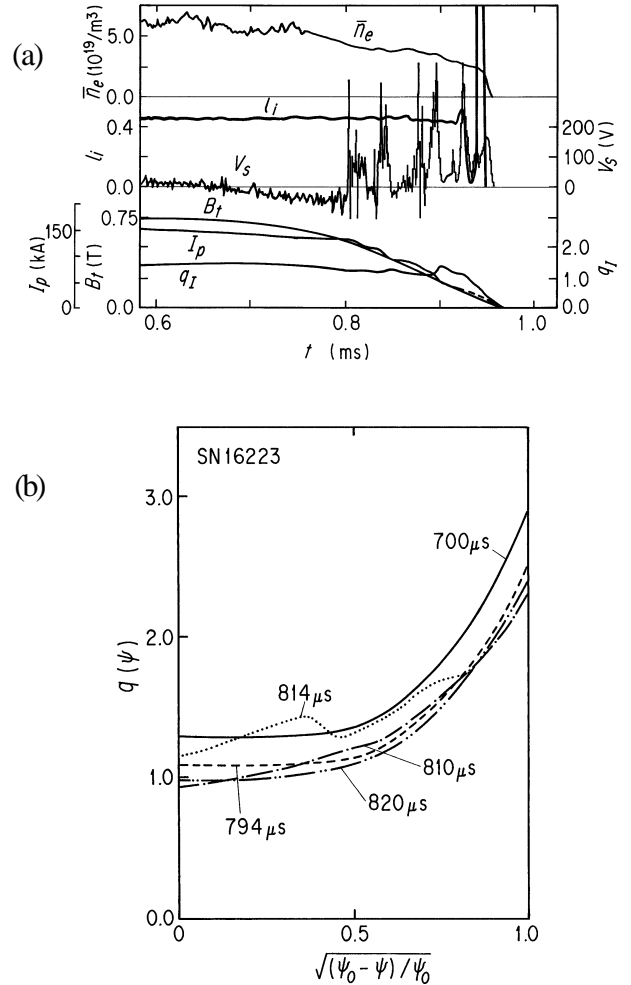


Fig.11 **a** B_t , I_p , q_I , V_s , l_i and \bar{n}_e are shown in B_t decaying phase. When B_t decreases from 0.7 ms in the low q plasmas ($q_I < 2$), I_p slightly decreases or remains constant even though V_s is negative. **b** The time variations of q profile near the low q limit are shown.

q decreases keeping the same shape of the relaxed state until q_I reaches the low q limit. In the figure, at 0.78 ms, the sampling time is changed from 0.2 μs to 1 μs . As l_i is calculated from the poloidal field profile and are averaged in 10 μs , l_i cannot correspond the fast change. Only the edge flux profile was slightly elongated. This means that the magnetic energy $1/2 L_i I_p^2$ is conserved during the time. That is, the q profile is conserved even though the edge q value decreases. B_t penetrates to the core plasma without any force. As the pointing vector is outward, the particles and plasma energy are lost. In the phase, $1/q_I$ increases with keeping $\bar{n}_e R/B_t$ constant. When q_I reaches the low q limit ($t=0.810$ ms), q profile

becomes broad and $q(0)$ becomes about 1. V_s decreases and I_p slightly increases, as the same as the case of $t=0.58-0.59$ ms in Fig.1 and Fig.9. $n=1$ mode grows and the reconnection may occur at $t=0.814$ ms. During the time, j_s increases at the edge region. A certain number of the energy and the particles are lost. After that, the plasma current decreases 20 % suddenly and $q(0)$ returns to above 1. The profile returns the original one ($t=0.82$ ms). This process repeats 3 ~ 4 times and I_p decreases step like so as to keep the minimum q_l of 1.2. On the step of I_p between the relaxations, the q and n_e profiles were almost the same as that of the relaxed state. The radiation loss power increases initially from the outer side of torus and finally the core radiation loss increases and the plasma decays.

As the relaxed profiles are reconstructed by the relaxation process, the current contraction, which leads to the major disruption, does not occur. The rotation speed increases at the relaxation phase, which is caused by the increase of the speed with decreasing of \bar{n}_e ¹⁰⁾. The locked modes do not appear.

§5 Error Field by An External Field

The current disruption does not occur in these short discharges with decaying phase of B_t . To excite the current disruption by the mode locking, the error field is added from the shell gap. In TPE-2, the shell is divided into 6 parts in the toroidal direction and into 2 parts in the poloidal direction. In the normal discharges, the auxiliary field is supplied to reduce the error field at the gap and to make the complete flux surface along the poloidal and the toroidal directions. When the auxiliary field (B_c) is reduced gradually, the error field increases in time. The time variations of B_t , I_p , V_s , q_l and \bar{n}_e were measured in the cases that B_c is enhanced properly and B_c is reduced, and are shown in **Fig.12a** and **13a**, respectively. The time variations of q profile near a relaxation transition of each case are shown in Fig.12b and 13b, respectively. The time variations of profiles of the poloidal magnetic field deformations ΔB_{ps} against

the poloidal angle: θ , were measured for the plasmas in both cases and are shown in Fig.12c and 13c, respectively. Here, B_{ps} is the peripheral poloidal magnetic field around the plasma and ΔB_{ps} is the deviation of B_{ps} from the relaxed one ($\bar{B}_{ps}(\text{relax})$), that is, $\Delta B_{ps}(=(B_{ps} - \bar{B}_{ps}(\text{relax}))/\bar{B}_{ps}(\text{relax}))$ ¹⁰⁾. ΔB_{ps} in the toroidal gap and on the inner surface of the shell are plotted. B_{ps} in the toroidal gap means the stray magnetic field from the shell gap. Where, the search coils for measurement of B_{ps} in the toroidal gap are placed outside of the inner surface of the shell. If B_c is proper, the shape of B_{ps} in the gap is nearly the same as B_{ps} on the inner surface of the shell.

In the case that B_c is proper, that is, in the case of without the error field, ΔB_{ps} on the inner surface of the shell and ΔB_{ps} in the shell gap rotate in the poloidal direction and rotated in the toroidal direction from the initial phase until the end of the discharge. Both profiles of ΔB_{ps} are almost the same during the discharge. The toroidal rotation was measured by the coils array of toroidal direction. In this figure, 2 relaxation phenomena are seen at $t=0.25$ ms and $t=0.62$ ms and \bar{n}_e decreases with steps. The q profile is almost the relaxed one (it is shown at $t=0.500$ ms, 0.640 ms in the figure) during the discharge except at the relaxation transition. At the relaxation transition, the q profile changes near $q=3$ surface, it is shown at $t=0.572-0.628$ ms, as $q(0)$ is larger than 2.

In the case that B_c is reduced in time and the other discharge conditions are same, that is, in the case with increasing the error field in time, the plasma gradually shifts to outer side of the torus by the decreasing of auxiliary compensation field. The humps near $\theta=0$ in the right of Fig. 13c are due to the shift. The q profile at $t=0.3$ ms is close to the relaxed one. However, it shrinks gradually and deviates largely from that of the relaxed one and $q(0)$ decreases gradually. Just after $q(0)<2$, an internal disruption occurs. The deformations on the surface of the shell and in the shell gap rotate at the initial phase, however, the rotating speed decreases gradually in the shell gap. After $t=0.2-0.3$ ms, the mode in the shell gap seems to stop, but the mode on the surface of the shell still rotates. From $t=0.45$ ms, the

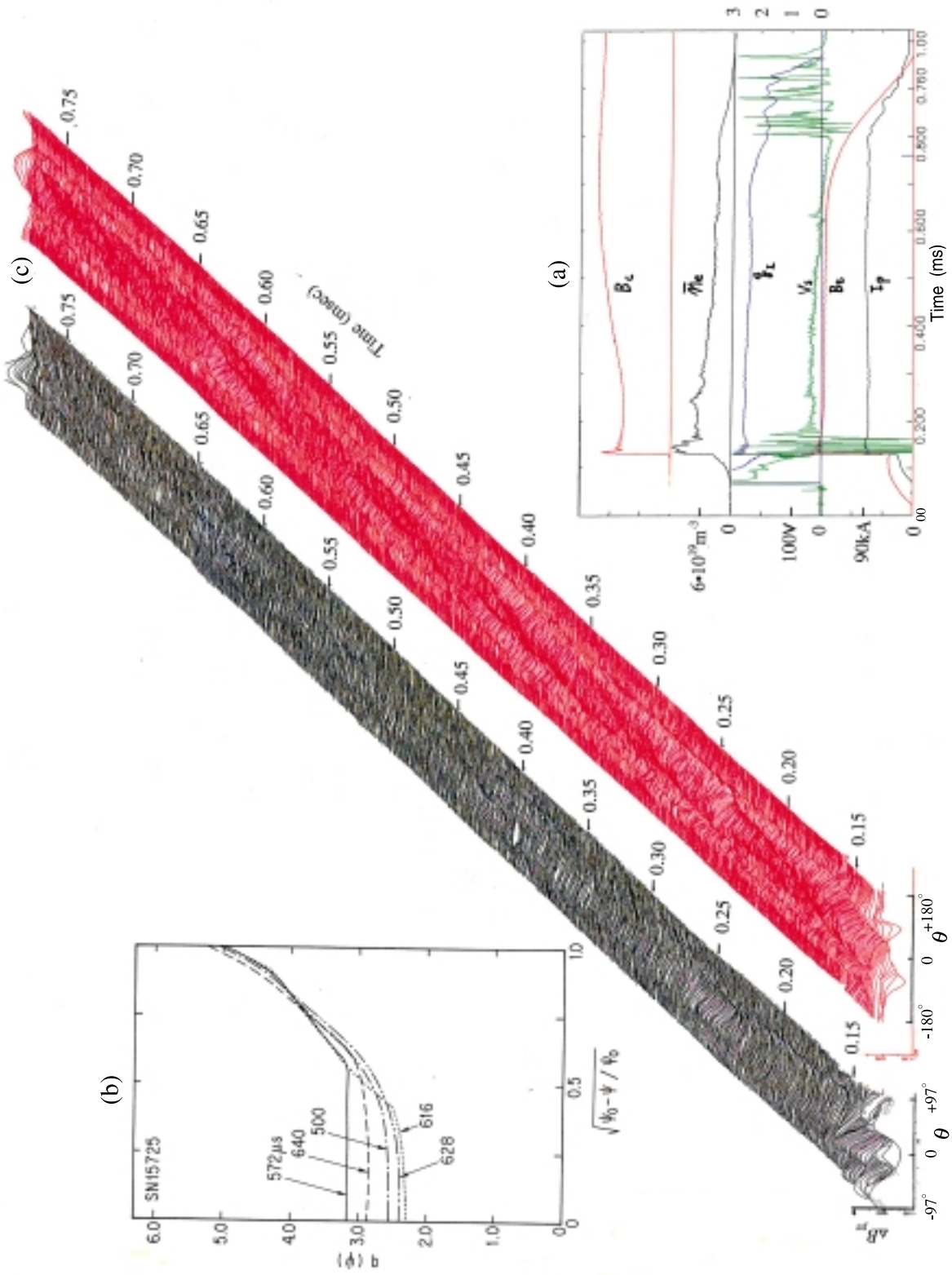


Fig.12 In a case without the error field at the shell gap, that is, in the case that B_c is proper. **a** The time variations of B_c , I_p , V_c , q_r , n_e and B_c are shown. **b** The time variations of q profile near a small relaxation transition are shown. **c** The time variations of profiles of the poloidal magnetic field deformations ΔB_p against θ are shown. ΔB_p in the shell gap (the left) and on the surface of the shell (the right) are plotted.

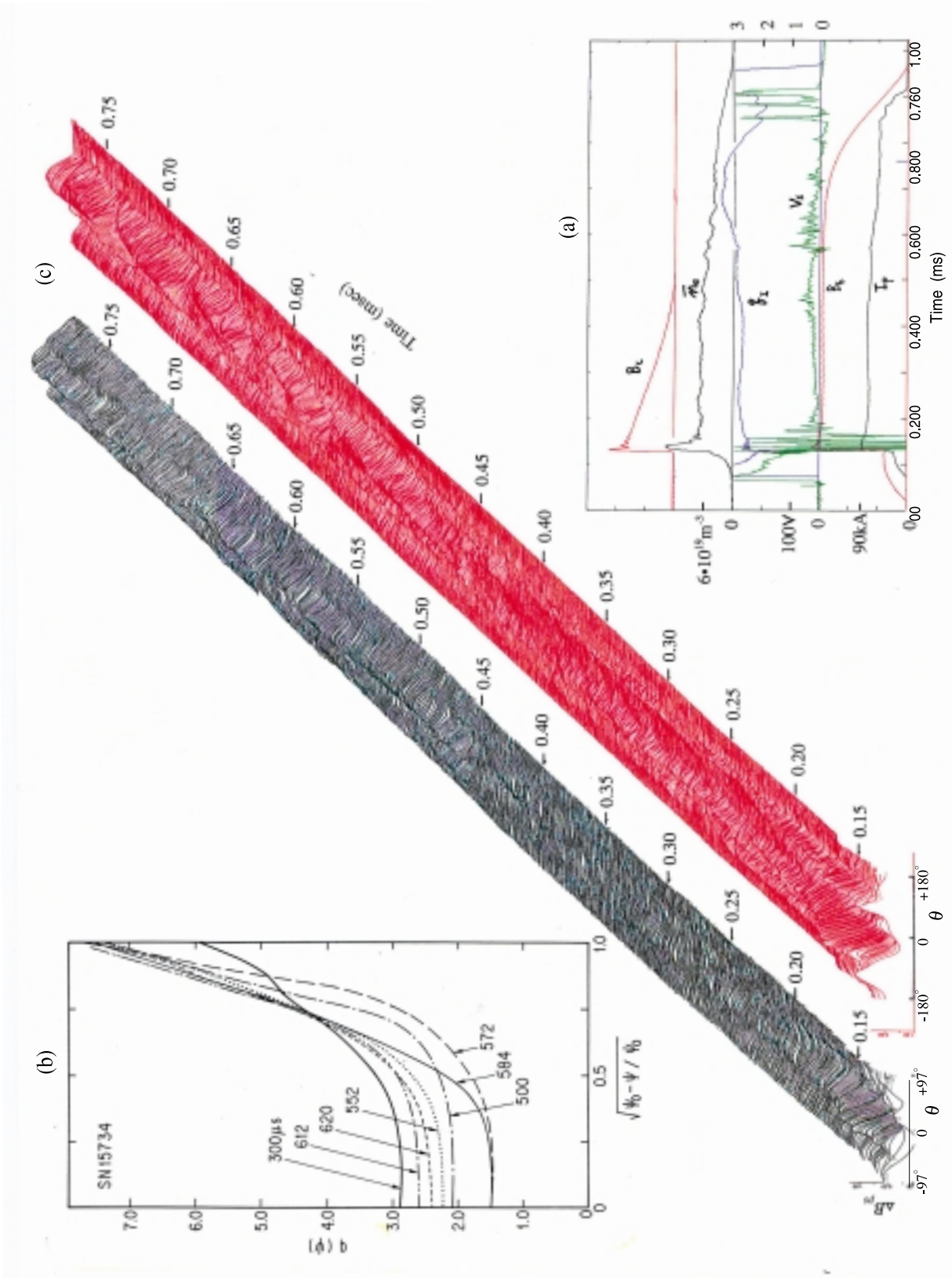


Fig.13 In a case with the error field at the shell gap, that is, in the case that B_z is reduced.
a The time variations of B_z , I_p , V_s , q , n_e and B_t are shown. **b** The time variations of profiles of the poloidal magnetic field deformations $\Delta B_{\theta s}$ against θ are shown. **c** The time variations of profiles of the poloidal magnetic field deformations $\Delta B_{\theta s}$ against θ are shown. $\Delta B_{\theta s}$ in the shell gap (the left) and on the surface of the shell (the right) are plotted.

rotating speed decreases and the $m=2/n=1$ mode grows. At $t=0.55$ ms, the internal disruption occurs and the current decays. The high particle and energy flows are observed at the outer side of the torus and \bar{n}_e decreases with steps.

The toroidal rotating times of the mode are measured and the velocities are estimated from the time. The toroidal rotating velocities on the surface of the shell just after the initial relaxation and just before the first internal disruption (for example, $t=0.25$ ms in Fig.12) are plotted against the normalized B_c in Fig.14 by \bullet and \blacktriangle , respectively. The rotating velocities in the shell gap just before the first internal disruption are also plotted by \circ . At first, the rotation stops in the shell gap and finally the velocity on the surface of the shell decreases about a half just before the first internal disruption. The friction at the shell gap may decrease the velocity in unperturbed region of inner side of the shell. After the internal disruption, $n=1$ mode rotates in the poloidal and the toroidal direction. As the error field is large, $n=1$ mode is not dumped by the rotation and the internal disruption occurs again just after the mode returns at the original place.

In conclusion, the error field may suppress the plasma

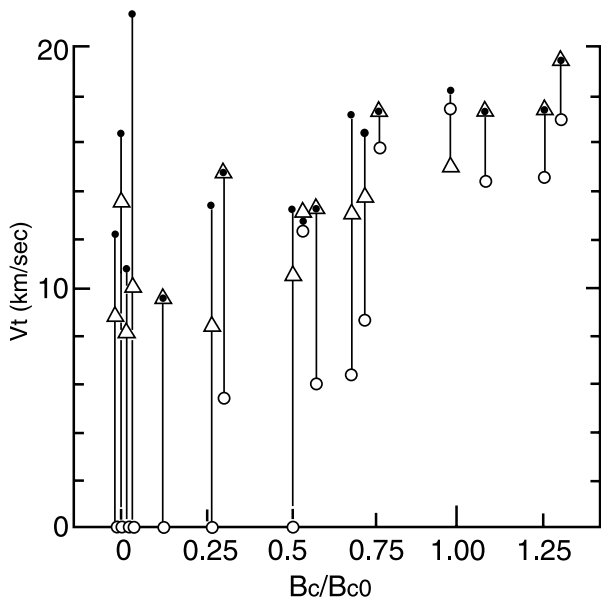


Fig.14 The toroidal rotation velocities on the surface of the shell at just after the initial relaxation and at just before the first internal disruption are plotted against the normalized B_c by \bullet and \blacktriangle , respectively. The velocities at the shell gap at just after the first internal disruption are plotted by \circ .

rotation near the toroidal shell gap at first, which causes the shrinking of the current distribution. Then, the internal disruption occurs at $q(0)<2$, that may be triggered by the $n=1$ mode.

§6 Discussions and Conclusion

In the high β low q tokamak experiment of TPE-2, the operation region related to the normalized density: $\bar{n}_e R/B_t$ and the normalized plasma current: $1/q_I$ exists. In the trace of $\bar{n}_e R/B_t - 1/q_I$ diagram, larger values of $\bar{n}_e R/B_t$ appear near $q_I=1.5-1.6$ and 3 and $\bar{n}_e R/B_t$ are minimum near $q_I=1, 2$ and 4, as shown in Figure 3. Highest value of $\bar{n}_e R/B_t > 0.7 \times 10^{20}/m^3$ ($\bar{n}_e > 1.2 \times 10^{20}/m^3$) are obtained only at $q_I \sim 3$, in which the Murakami law determines the density limit. The values of $\bar{n}_e R/B_t$ are same as that of the usual tokamaks. However, the values of the other region are extremely less than of the tokamaks. A linear dependence of $\bar{n}_e R/B_t$ on $1/q_I$ of the maximum density is not clear. The current disruption by the Hugill density limit was not observed, because of the discharges without gas puff, of the low recycling surface and of the short discharge duration. The trace is different from the Hugill diagram for the usual tokamaks, in which the densities are increased by gas puff and the current disruption occurs in high-density regions. The high Murakami number at $q_I \sim 3$ may be due to the high power plasma production by the implosion heating at high Murakami number and the effect of the enhanced Ohmic heating in low aspect ratio and elongated cross-section.

The particle confinement at the edge related to q_I determines the maximum density, because the outflow of the particles: \bar{j}_s/\bar{n}_e are minimum at $q_I \sim 1.5-1.6$ and 3, as shown in Fig.4, furthermore, the influx of the particles, \bar{D}_α/\bar{n}_e are minimum in the windows. The particle loss at the relaxation mainly results in the density decay, as shown in Fig.1.

The dependence of \bar{n}_e (or $\bar{n}_e R/B_t$) on $1/q_I$ may be due to the period of the relaxation oscillation, as shown in Fig.10. The sharp decrease of \bar{j}_s/\bar{n}_e at $q_I \sim 1.5-1.6$ and 3 may be due to MHD stabilities. In this plasma, in the

case of $q_I \sim 1.5-1.6$, $q(0)$ (30 % ψ) is nearly 1.5, that is, above 1, and in the case of $q_I \sim 3$, $q(0)$ is nearly 3, that is, above 2. The internal disruption does not occur because $q(0)$ is far from 1 or 2. In the case of $q_I \sim 1.5-1.6$, the $m=6/n=3$ ballooning-like mode rotates in the toroidal and the poloidal direction¹⁴⁾. When the mode break to $m=2/n=1$ mode at the edge region the relaxation oscillation occurs. If the intensity of the $m=2/n=1$ mode is small, the relaxation oscillation or the reconnection was local, then the local measurement could not observe the events sometimes. For example, the density decreases abruptly without the sign of magnetic fluctuations at the same measurement point, but that appear at the opposite point. This caused the scatters of the data in Fig.3 and 4. Then, we measured the averaged density, \bar{n}_e , or outflow of the particle \bar{j}_s/\bar{n}_e . The ideal MHD modes for this plasma were calculated by ERATO code and $n=1, 2$ and 3 modes are stable but $n=\infty$ ballooning mode is unstable in the edge plasma¹⁴⁾, when $q_I \sim 1.5-1.6$. We understand the plasma rotation suppress the growth of the MHD instabilities. We suppose the long period of the relaxation oscillation at $q_I \sim 1.5-1.6$ and 3 is due to that $q(0)$ is far from 1 or 2.

Between the relaxation oscillations the density profile is rather sharper and it is due to that the particle outflow is suppressed in the edge region and particle confinement of the core plasma increase. \bar{n}_e decrease slightly between relaxations. The particle losses may be caused by the low n ballooning mode. The density decays slightly at the local region by the mode.

The minimum of \bar{n}_e (or $\bar{n}_e R/B_t$) near $q_I \sim 1$ and 2 may be due to the internal disruption at $q(0) \sim 1$ and 2 .

In the region of $2 > q_I > 1.6$, \bar{j}_s/\bar{n}_e is quite higher than that of $q_I \sim 1.5-1.6$, however, \bar{n}_e (\bar{j}_s/\bar{n}_e) is not so lower than that of $q_I \sim 1.5-1.6$, as shown in Fig.3. The density profile becomes broad near $2 > q_I > 1.8$, as shown in Fig.5b. One reason is that the plasma of $2 > q_I > 1.7$ is generally produced in the ramp up mode, the effect of the violent relaxation at the transition of $q_I=2$ remains, that is, the plasma after mild relaxation can only enter to $q_I < 1.6$ and stay with rather good particle confinement. In the case of the plasma after the violent relaxation,

many particles and the considerable part of internal energy are lost, then \bar{n}_e and β become low, and the plasma cannot enter $q_I < 1.6$.

$\bar{n}_e R/B_t - 1/q_I$ traces in the initial time of the discharges move roughly in the operation regions, as shown in Fig.3. The high Murakami numbers are obtained generally in the low q mode and the high q mode, in which modes q_I are nearly 1.5-1.6 and 3 after the initial relaxation and the period of the relaxation oscillation is longer. Then, to avoid the particle loss, the plasmas should be produced in the windows near $q_I=1.5-1.6$ and 3 from the initial discharge until the end of the discharge.

$q_I=1.2$, which is the low q limit in this experiment, was achieved only in low-density plasma. The lowest q is higher than 1.2 in high-density plasma. The internal particles and energy are lost from the edge plasma at the limit. The plasma current decreases a few %, and then q_I stays above the low q limit. In the B_t decaying phase, $1/q_I$ increases with constant $\bar{n}_e R/B_t$. The pure plasma current disruption, which is observed in the usual tokamaks, does not occur, even though a number of the particles and the energy are lost. As the rotation speed increases with $1/q_I$ and with decreasing of \bar{n}_e and with decreasing recycling rate, there is no cause to make the mode locking in this experiment. Then, the disruption by the mode locking does not occur. The plasmas disappear at the low q limit keeping a high rotation speed in B_t decaying phase.

In order to stop the rotation, an error field was supplied to the toroidal shell gap. At first, the error field may suppress the plasma rotation from the shell gap and causes the shrinking of the current distribution and then causes the internal disruption at $q(0) \sim 2$. The plasma rotation is important to avoid the disruption as same as the usual tokamaks. The mode locking may be easy to occur in plasmas with gas puff. To avoid this type of disruption, the low recycling wall and the proper gas puff rate are suitable.

In the slow screw pinch mode, \bar{n}_e increases with constant $\bar{n}_e R/B_t$ after the initial relaxation. It is due to that the particle confinement increases with B_t . The density of the pre-heat plasma decreases suddenly due

to bad confinement because of no compensating field. Then, the exited neutral atom near the wall may be ionized during B_t and I_p ramp up time, then \bar{n}_e increases with B_t .

In this paper, we used the averaged values of \bar{n}_e , \bar{j}_s , and global out flow velocity: \bar{j}_s/\bar{n}_e to understand the Hugill diagram and the operation region of the high β low q tokamak plasma. In the averaging time, relaxation phenomena are included. \bar{j}_s/\bar{n}_e without the relaxation becomes small even in the region except the windows and the operation region expands. For example, the decay time of \bar{n}_e was about 0.6 ms, while that of \bar{n}_e without relaxation was 1-5 ms. But, this is no meaning to understand the operation region because the relaxation or the reconnection phenomena occur always, which depend on mainly q_I . This is the feature of the high β low q tokamak plasma.

The energy confinement time: τ_E of the high q mode (in this figure, $q_I \sim 3$) and the ramp up mode ($q_I \sim 1.5-1.6$) are shown in **Fig.15**a, b. τ_E increases with the density,

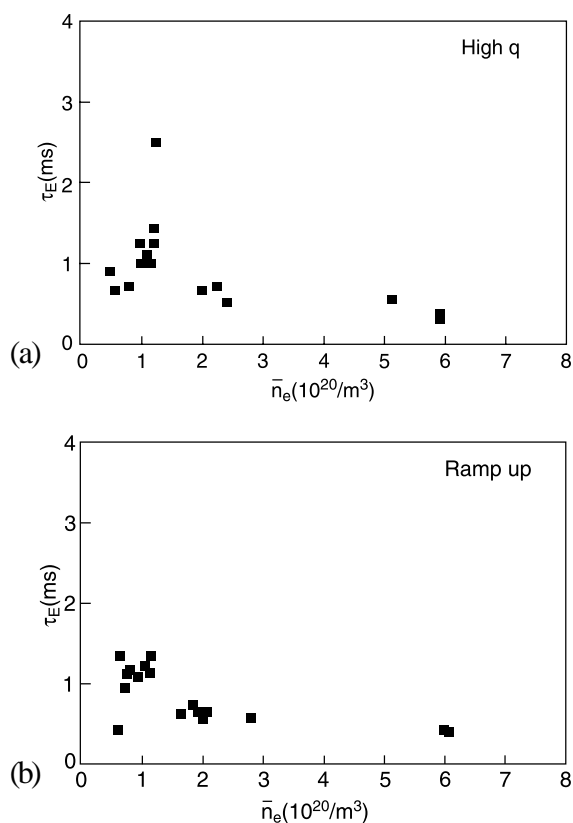


Fig.15 The energy confinement time: τ_E are plotted against \bar{n}_e . **a** The high q mode. **b** The ramp up mode.

but it becomes peak near $\bar{n}_e \sim 1.2 \times 10^{20}/m^3$ and decreases with increasing the density. τ_E is about 1 ms. The recycling increases above the value of the density, as shown in Fig.7c and 8a. The energy confinement decreases with the high recycling plasma.

In conclusion, in the high β low q tokamak plasmas, there are windows for the density at $q_I = 1.5-1.6$ and 3 in the $\bar{n}_e R/B_t - 1/q_I$ traces. The particle losses at the relaxation phenomena mainly determine the dependence. The error field at the shell gap restrains the plasma rotation at the place, causes the current shrinking, and then gives rise to the current disruption.

References

- 1) M. Murakami, J.D. Callen and L.A. Berry : Nucl. Fusion **16** (1976) 347.
- 2) P.E. Stott, J. Hugill, S.J. Fielding, et al. : *Proc. 8th EPS Conf. on Controlled Fusion and Plasma Physics, Prague, 1979*, Vol. 1 (European Physical Society, Prague, 1979) 151.
- 3) M. Greenwald, J.L. Terry, S.M. Wolfe, S. Ejima, M.G. Bell, S.M. Kaye and G.H. Neilson : Nucl. Fusion **28** (1988) 2199.
- 4) J.A. Wesson, R.D. Gill, M. Hugon, F.C. Schuller, J.A. Snipes, D.J. Ward, D.V. Bartlett, D.J. Campbell, P.A. Duperrex, A.W. Edwards, R.S. Granetz, N.A.O. Gottardi, T.C. Hender, E. Lazzaro, P.J. Lomas, N. Lopes Cardozo, K.F. Mast, M.F.F. Nave, N.A. Salmon, P. Smeulders, P.R. Thomas, B.J.D. Tubbing, M.F. Turner and A. Weller : Nucl. Fusion **29** (1989) 641.
- 5) S. Kiyama, H. Ashida, K. Hayase, I. Hirota, N. Ikeda, H. Kiyama, Y. Maejima, Y. Satoh, M. Kito, S. Takeda, E. Yahagi and T. Tamaru: *Proc. of 10th Inter. Conf. on Plasma Physics and Controlled Nuclear Fusion Research, London, 1984*, Vol.1, (IAEA, Vienna, 1989) p.393.
- 6) S. Kiyama, H. Ashida, I. Hirota, H. Kiyama, Y. Maejima, Y. Satoh, S. Takeda, K. Hayase, E. Yahagi and M. Kito : Bull. Electrotech. Lab. **50** (1986) 451.
- 7) K. Hayase, I. Hirota, S. Kiyama, H. Kiyama, Y. Maejima, Y. Satoh, S. Takeda, E. Yahagi and M. Kito : *Proc. of 11th Inter. Conf. on Plasma Physics and Controlled Nuclear Fusion Research, Kyoto, 1986*, Vol.2 (IAEA, Vienna, 1989) p.563.
- 8) H. Kiyama, K. Hayase, I. Hirota, S. Kiyama, Y. Maejima, Y.

Satoh, S. Takeda, E. Yahagi and M. Kito : *Proc. of 12th Inter. Conf. on Plasma Physics and Controlled Nuclear Fusion Research, Nice, 1988, Vol.1* (IAEA, Vienna, 1989) p.437.

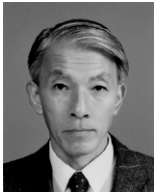
- 9) S. Kiyama, H. Ashida, I. Hirota, H. Kiyama, Y. Maejima, Y. Satoh, S. Takeda, K. Hayase and M. Kito : Electrotech. Lab. Report 937, March 1992.
- 10) H. Kiyama : Bull. Electrotech. Lab. **55** (1991) 1227.
- 11) H. Kiyama : Bull. Electrotech. Lab. **56** (1992) 303.
- 12) H. Kiyama and S. Kiyama : *Proc. of 1992 Inter. Conf. on Plasma Physics, Innsburg, 1992, Vol.2*, 799.
- 13) H. Kiyama and S. Kiyama : *Proc. of 20th EPS Conf. on Controlled Fusion and Plasma Physics, Lisboa, 1993, Vol.2*, 687.
- 14) H. Kiyama and S. Kiyama : Nucl. Fusion **36** (1996) 1221.
- 15) H. Kiyama and S. Kiyama : Bull. Electrotech. Lab. **58** (1994) 9.

(Accepted June 15)

Author



Hiroko KIYAMA
Energy Technology Division
E-mail : kiyamah@etl.go.jp
The author works on plasma physics and controlled nuclear fusion research.



Satoru KIYAMA
Energy Technology Division
E-mail : kiyamas@etl.go.jp
The author works on plasma physics and controlled nuclear fusion research.